Environmental Science Processes & Impacts

ROYAL SOCIETY OF CHEMISTRY

PAPER

View Article Online
View Journal | View Issue

Open Access Article. Published on 06 Februarie 2026. Downloaded on 2026-05-11 6:57:09 nm..
This article is licensed under a Creative Commons Attribution-NonCommercial 3.0 Unported Licence.

Check for updates

Cite this: *Environ. Sci.: Processes Impacts*, 2026, **28**, 752

Accelerated O_3 formation triggered by summer heatwaves in megacity Seoul

Junsu Gil,[ab] Meehye Lee,*[ac] Moon-soo Park,[d] Cheol-Hee Kim,[e] Ja-ho Koo,[f] Hyojung Lee,[e] Sunggu Kang[a] and Hojoon Rhee[ag]

Received 12th August 2025
Accepted 9th January 2026

DOI: 10.1039/d5em00629e

rsc.li/espi

As compelling evidence of global warming, heatwaves are expected to elevate O_3 mixing ratios in highly polluted urban areas. In summer 2018, Seoul, an Asian megacity, experienced elevated O_3 levels in conjunction with a temperature surge (maximum of 38.9 °C). This study quantitatively estimates the O_3-climate penalty through measurements of nitrogen oxide species, volatile organic compounds (VOCs), and the boundary-layer height, as well as model simulations. The results highlight an acceleration of O_3 concentration increment with increased temperature and elevated ozone production efficiency in NO_x-saturated conditions. Furthermore, it emphasizes the importance of dynamic boundary-layer processes and increased VOC concentrations resulting from fugitive emissions during the heatwave.

Environmental significance

With global warming, surface ozone levels are expected to increase with more frequent heatwaves, but the detailed process of interaction between ozone and heatwaves is still unclear. In summer 2018, we observed an ozone enhancement in conjunction with an extreme heatwave, quantified its temperature dependency, and elucidated its driving processes. We found that reinforced vertical mixing of air mass with the additional fugitive emission of volatile organic compounds in the reactive nitrogen oxide saturated megacity plays a key role in boosting ozone production efficiency increase, and it accelerates the daytime ozone enhancement. This implies that more frequent heatwaves due to climate change could induce faster and greater ozone increases in megacities than expected.

1. Introduction

Numerous spatiotemporal observations and modeling studies indicate an ongoing and projected continuous increase in global surface temperature.[1] Under the worst-case scenario of the Shared Socioeconomic Pathways (SSPs), the rise in climate change pollutants could cause a significant increase in global temperature. For example, climate simulation models project a rise in average temperature up to 7.0 °C in Northeast Asia by 2100.[2–4] This temperature surge is anticipated to elevate O_3 mixing ratios, particularly in urban areas with high emissions of NO_x and volatile organic compounds (VOCs) under extreme meteorological conditions. Notably, O_3 concentrations spiked during the 2018 heatwaves in European and Asian cities.[5–10] This drew attention to O_3 as both a short-lived climate pollutant (SLCP) contributing to global warming[11–13] and a key air pollutant deteriorating air quality.[14]

To recognize the positive feedback between surface O_3 and global warming, a comprehensive understanding of the interplay between chemical ozone production mechanisms and climate variables is imperative. In recent years, increases in surface O_3 due to climate change have been labeled the "O_3-climate penalty", underscoring this gas' adverse impacts on the climate system and the associated costs of climate change mitigation and damage repair measures.[15,16] Recent studies have suggested methods for quantifying the O_3-climate penalty as an "O_3-climate penalty factor" (CPF_{O_3}) using statistical fitting[17–19] or discretization methods combined with model simulations.[20–22] Despite the various factors that influence O_3 increase across different regions, the CPF_{O_3} calculated from long-term measurement data is quite similar in most areas, particularly at background sites (0.1–3.2 ppbv $°C^{-1}$).[16,21,23]

As global warming intensifies, megacities around the world are experiencing increased O_3 levels during heatwaves.[24] These extreme events are clear indicators of global warming and highlight the urgent need for research to explore the mechanisms and key factors contributing to elevated O_3 levels during heatwaves. In summer, the chemical reactivity linked to precursor emissions is significantly increased. Therefore, in this season, the chemical processes driving O_3 formation tend

[a]Department of Earth and Environmental Sciences, Korea University, Seoul, South Korea
[b]Institute of Basic Sciences, Korea University, Seoul, South Korea
[c]Graduate School of Energy and Environment, Korea University, Seoul, South Korea
[d]Department of Climate and Environment, Sejong University, Seoul, South Korea
[e]Department of Atmospheric Sciences, Pusan National University, Pusan, South Korea
[f]Department of Atmospheric Sciences, Yonsei University, Seoul, South Korea
[g]Seoul Metropolitan Government Research Institute of Public Health and Environment, Seoul, South Korea

This journal is © The Royal Society of Chemistry 2026

Open Access Article. Published on 06 Februarie 2026. Downloaded on 2026-05-11 6:57:09 nm..
This article is licensed under a Creative Commons Attribution-NonCommercial 3.0 Unported Licence.

to outweigh the physical processes associated with its long-range transport, which can lead to a pronounced increase in CPF_{O_3} in urban areas.[25]

Various studies have shown a correlation between O_3 formation and temperature in polluted regions during short-term heatwaves,[26–28] suggesting that O_3 formation reinforced over time. Given the significant impact of O_3 on human health, its accelerated formation due to temperature rise can lead to dangerously high levels, posing serious risks to residents of megacities.

Seoul, a megacity in South Korea, experienced an extreme heatwave in summer 2018, which saw an unprecedented daily maximum temperature exceeding 38 °C accompanied by a significant increase in O_3. Since 2000, Seoul has witnessed a continuous annual increase in the 99th percentile temperature of 0.09 °C per year and in the annual average O_3 concentration of 1.28 ppbv per year (Fig. 1). These variations of 99%ile O_3 concentration and temperature value represent the changes in summer season, when the O_3 level is strongly determined by the photochemical reaction. The 2018 heatwave caused the rate of increase in the annual average temperature and O_3 to rise to 0.15 °C per year and 1.73 ppbv per year, respectively,[29] approximately 67% and 54% larger than before the heatwave. The exceptionally high temperatures recorded during the 2018 heatwave exemplify the effects of climate change[30–32] and resulted in surface O_3 concentrations exceeding South Korean air quality standards.[33] These observations suggest that, in the future, the rise in extreme temperatures due to global warming may cause critical O_3-related challenges in megacities, similar to those observed during the 2018 heatwaves.

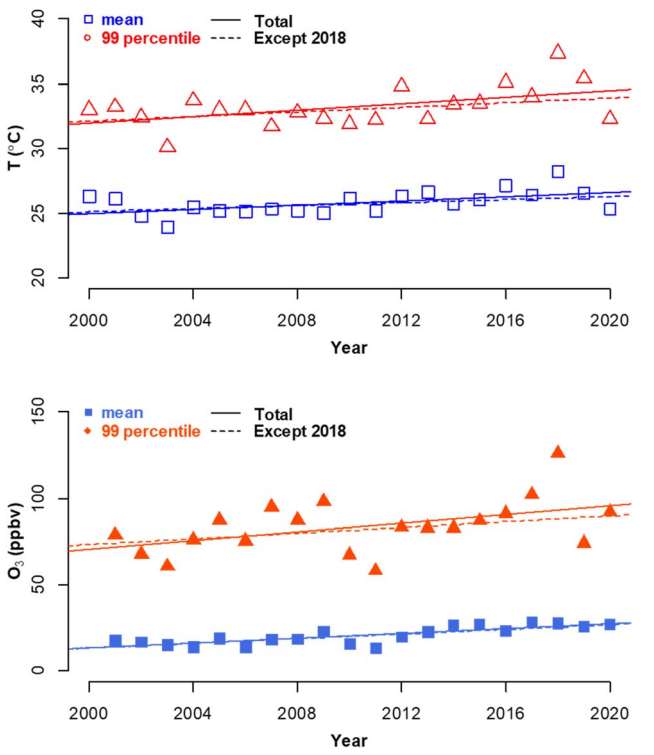

Fig. 1 Annual mean variation (blue square) and annual maximum variation (red triangle) of the atmospheric temperature (open symbol) and surface O_3 (solid symbol) during the hot-summer (Jul–Aug) at Jongro-gu in Seoul, South Korea (data are from the Korea Meteorological Administration and Korea Ministry of Environment website). The dashed linear regression line describes the annual variation until 2020, and solid linear regression line implies the change of annual variation when add the 2018 data.

This study aimed to estimate the CPF_{O_3} during a short heatwave in a highly polluted urban area in Seoul and explore the crucial factors determining this parameter using observational data and model results obtained in the summer of 2018. The findings provide vital information for policies to abate O_3 pollution and for addressing emerging challenges in megacities during heatwaves, potentially intensified by future warming.

2. Materials and methods

2.1. Field measurements

All measurements were conducted between 13 July and 20 August 2018 in urban Seoul, South Korea. Trace gases and aerosol composition were measured at the Korea University campus (KU, 37.59° N, 127.03° E, 27 m a.g.l.). Additionally, 55 VOC species and vertical winds were measured in the districts of Jongro-gu (37.57° N, 127.01° E) and Jungnang-gu (37.59° N, 127.08° E, 22 m a.g.l.), located near KU (Fig. S1).

O_3, NO, and NO_2 were measured using commercial instruments—respectively, a 49i, Thermo Scientific; a 42i, Thermo Scientific; and a T500U, Teledyne API. The detection limits of these instruments were 1, 0.4, and 0.04 ppbv, respectively.

The mixing ratios of 55 VOCs were measured in real-time using an automatic gas chromatography-flame ionization detector (GC-FID; Clarus 500, PerkinElmer) with a Thermal Desorption (TD; TurboMatrix 300, PerkinElmer) unit. Ambient air samples (600 mL) were collected using a small pump for 40 min at a flow rate of 15 mL min^{-1}. The pump was controlled by a mass flow controller. A Nafion dryer was used to remove water from each sample, and the VOCs in the moisture-depleted sample were concentrated at −30 °C in a cold trap using a thermal desorption unit. Then, the temperature of the trap was rapidly increased to >300 °C to induce desorption, and the desorbed sample was transferred to the high-resolution capillary column of the GC-FID through a transfer line with high-purity nitrogen carrier gas. Each desorbed sample was separated through two columns, one polar (plot column) and one non-polar (bp-1 column), before the VOCs were detected by the FID.

Peroxyacetyl nitrate (PAN, $CH_3COO(O)NO_2$) was measured using gas chromatography-luminol chemiluminescence detection (GC-LCD).[34,35] A 10 m capillary column (DB-1, Agilent, USA) was used and a photomultiplier tube (HC135-01, Hamamatsu, USA) was connected to the reaction cell where the luminol solution and PAN were mixed. The height of the PAN peak was quantified using a Molybdenum-NO_x instrument (T500U, Thermo Scientific). The PAN standard was formed by reacting with vaporized liquid acetone with standard NO_2 gas under UV light in a chamber. Data was ensembled into one-hour data every two minutes.

The HONO concentration was measured using a parallel-plate diffusion scrubber coupled with an ion chromatography (PPDS-IC) system. Ambient air was sampled slowly (0.8 L min^{-1}) through a 1 m long 1/4″ PTFE tube and was solubilized in the collected solution (deionized water, HPLC grade, J. T. Baker) by

Open Access Article. Published on 06 Februarie 2026. Downloaded on 2026-05-11 6:57:09 nm..
This article is licensed under a Creative Commons Attribution-NonCommercial 3.0 Unported Licence.

penetrating a membrane filter (0.2 μm pore size, Osmoncis) in the PPDS. The collected solution was injected into the analysis column (AS14, Dionex IonPac™) with an eluent solution (3.5 mM Na_2CO_3, $NaHCO_3$ mixed solution). The time resolution of the HONO and HNO_3 measurements was 15 min, and hourly average data were used for the analysis. The detection limit was 20 pptv. Details of the measurement and calibration methods are provided in previous paper.[36]

A ceilometer (CL51, Vaisala) was used to obtain vertical profiles of backscattering coefficients at intervals of 10 m to 15.4 km using a laser (InGaAs diode laser) with a wavelength of 910 nm.[37] A wind lidar (Windcube-200, Leosphere) was used to measure the vertical profile of wind speed and direction using a Doppler beam swinging scanner with a 1532 nm wavelength laser.[38] A microwave radiometer (MWR) was used to observe the atmospheric attenuation and brightness temperature based on electromagnetic radiation emitted from the atmosphere using 14 channels (seven channels between 22 and 31 GHz for water vapor, seven channels between 51 and 58 GHz for temperature).[39] This instrument measures two types of temperature profiles: zenith scanning for the entire troposphere (0–10 km) and elevation scanning for the boundary layer (0–2 km). The atmospheric boundary-layer height was estimated with the Integrated System for Atmospheric Boundary Layer height Estimation (ISABLE) algorithm using the vertical profile of the backscatter coefficient obtained from a ceilometer and the vertical temperature profile obtained by a MWR.[40]

2.2. Model simulations

This study employed an open-source box model (For 0-D Atmospheric Modelling, F0AM) to conduct a sensitivity test of O_3 precursors in response to temperature changes using measurement data. The F0AM, developed by Wolfe *et al.* (2016), is suitable for modeling changes in atmospheric pollutants under biogenic influence.[41] By applying the Master Chemical Mechanism (MCMv3.3.1), the F0AM model effectively estimates the variation in O_3 levels in response to changes in temperature and concentrations of precursor gases such as NO_x and VOCs.

To facilitate the calculations, the OH reactivity of all VOCs (Table S1) was assessed and the top 10 VOCs were selected (Table S2), which accounted for 70% of the total OH reactivity. In the model simulations, the average diurnal O_3 variation profile was calculated using the measurement data, and the modeled value was optimized using a daily maximum O_3 concentration as the criterion. Since *m*,*p*-xylene could not be distinguished, it was treated as *m*-xylene in the simulation. Following the model optimization process, the bias of the results was under 1.1 ppbv, with the uncertainty attributed to *m*,*p*-xylene being estimated at approximately 0.4 ppbv.

For testing the changes in temperature, NO_x, and VOCs to the daily maximum O_3 concentration, we controlled each parameter following under conditions.

M_T: other parameters in the model were fixed and only the temperature was changed. Two SSPs were used (SSP1 and SSP5), conditions in which the temperature increased every hour following the SSP results (SSP1: +2.6 °C and SSP5: +7.0 °C) of previous studies.[2,3] The M_A–M_S scenario was simulated based on these temperature change condition.

M_A: increasing the VOCs (excluding isoprene) from anthropogenic sources ("AVOCs"). Incremental ratio of AVOCs is set to 1.3% $°C^{-1}$,[42] considering the emission characteristics in this region that vehicle sources are dominant.[43]

M_B: isoprene (C_5H_8) was selected as a representative VOC from biogenic sources ("BVOC"). Its increase ratio was calculated using the temperature response factor (Table S6), which is discussed elsewhere.[44,45]

M_N: the temperature dependency of NO_x is not well understood; therefore, NO_x was considered to have originated from anthropogenic vehicle emissions, and the increase ratio was set to 1.3% $°C^{-1}$ (*i.e.*, the same as that used for AVOCs).[27,46]

M_S: all variables (AVOCs, isoprene, and NO_x) were changed.

Additionally, the Weather Research and Forecasting model coupled with Chemistry (WRF-Chem) v3.9.1 was used to simulate the variation in O_3 and VOC concentrations during both heatwave and non-heatwave periods. The WRF-Chem (version 3.9.1) model[47,48] was used to simulate O_3 and other atmospheric pollutants, including $PM_{2.5}$, SO_2, and NO_2, during both heatwave and non-heatwave periods. The model domain encompassed Northeast Asia (105–145° E, 25–50° N) and was configured with a grid spacing of 27 km and 28 vertical layers extending from the surface to 50 hPa. Meteorological initial and boundary conditions were sourced from the National Center for Environmental Prediction Final (NCEP/FNL) Operational Global Analysis data,[49] which have a horizontal resolution of 1° × 1°. The Regional Atmospheric Chemistry Mechanism (RACM)[50] was used for the gas-phase chemical scheme and the Modal Aerosol Dynamics Model for Europe/Volatility Basis Set (MADE/VBS)[51] for the aerosol scheme. Biogenic emissions were derived from the Model of Emissions of Gases and Aerosols from Nature (MEGAN) version 2.04,[45] while anthropogenic emissions were obtained from the KORUSv5 emission inventory, which was developed by a joint research group from Konkuk University and the National Institute of Environmental Research for the 2016 KORea-United States Air Quality (KORUS-AQ) field campaign.[52] The physical and chemical model options used in this study are summarized in Table S3.

2.3. O_3-climate penalty and CPF_{O_3}

Multiannual observation studies have found that O_3 levels increase with rising temperature. While the sensitivity of O_3 to temperature change is consistent in long-term observations, variability has been reported in short-term measurements.[26,53,54] The relationship between O_3 and temperature change is often expressed using linear regression or quadratic equations to capture changing dynamics. Based on the quadratic regression curve relating O_3 and temperature ($[O_3]_{max} = b_0 + b_1[T]_{max} + b_2[T]_{max}^2$), the CPF_{O_3} can be defined by the slope of the quadratic curve ($2b_2$), and the O_3–temperature dependency $\left(\frac{d[O_3]_{max}}{d[T]_{max}}\right)$ can be calculated using the following equation (eqn (1)):

$$\frac{d[O_3]_{max}}{d[T]_{max}} = 2b_2[T]_{max} + b_1 \quad (1)$$

 This journal is © The Royal Society of Chemistry 2026

Open Access Article. Published on 06 Februarie 2026. Downloaded on 2026-05-11 6:57:09 nm..
This article is licensed under a Creative Commons Attribution-NonCommercial 3.0 Unported Licence.

However, accurately estimating the O_3 variation caused by increasing temperature is challenging due to multiple influencing factors, including physicochemical changes and anthropogenic–biogenic emissions related to temperature increase. The response of O_3 to temperature can be assessed through (i) direct methods that examine the relationship between the observed O_3 concentration and temperature, and (ii) indirect methods that analyze how temperature impacts various O_3-influencing factors.[55–57] Definitions of the O_3-climate penalty vary across studies, with some using the slope of O_3 concentration *versus* temperature[16] and others deriving it from the results of chemical transport models related to increases in anthropogenic emissions.[15] Rasmussen *et al.* (2013) proposed the following equation (eqn (2)) to express the indirect relationship between O_3 concentration and temperature:

$$\frac{d[O_3]}{dT} = \frac{d[O_3]}{d(Phy)} \times \frac{d(Phy)}{dT} + \frac{d[O_3]}{d(Chem)} \times \frac{d(Chem)}{dT} + \frac{d[O_3]}{d(Emi)} \times \frac{d(Emi)}{dT} + \cdots = \left.\frac{d[O_3]}{dT}\right|_{Phy} + \left.\frac{d[O_3]}{dT}\right|_{Chem} + \left.\frac{d[O_3]}{dT}\right|_{Emi} + \cdots \quad (2)$$

where d(Phy) represents the change in physical processes (*e.g.*, stagnation or transport of air masses), d(Chem) refers to the changes in chemical parameters affected by temperature (*e.g.*, reaction rate constants), and d(Emi) indicates the variation in precursor emissions with rising temperature.[20] Other factors influencing the O_3–temperature relationship, such as relativity humidity, have a negligible impact in urban areas.[20,58] The terms $\left.\frac{d[O_3]}{dT}\right|_{Phy}$, $\left.\frac{d[O_3]}{dT}\right|_{Chem}$, and $\left.\frac{d[O_3]}{dT}\right|_{Emi}$ were estimated by considering the change in atmospheric chemical conditions and synoptic meteorology, allowing the sensitivity of O_3 to temperature changes during heatwaves in a megacity to be determined.

3. Results and discussions

3.1. Estimation of the O_3-climate penalty factor

During the measurement period, there were 29 days of heatwaves according to the South Korean criteria, which defines a heatwave as a daily maximum temperature exceeding 33 °C. During this time, an extremely high temperature of 38.9 °C was recorded under blocking conditions over the Korean Peninsula (Fig. S2).[30–32] On eight days during this high-temperature period, high-O_3 episodes occurred which exceeded the national ambient air quality standard (hourly average O_3 concentration of >100 ppbv). Throughout the heatwave period, the average O_3 concentration was 36.6 ppbv, with a daily maximum of up to 169.4 ppbv. Additionally, the average and daily maximum O_3 levels were higher than in the non-heatwave period by approximately 9 and 54 ppbv, respectively. Ozone levels consistently increased with rising temperatures throughout the measurement period, with the most significant increase observed during the heatwave period, as is clear from the daily maximum values (Fig. 2).

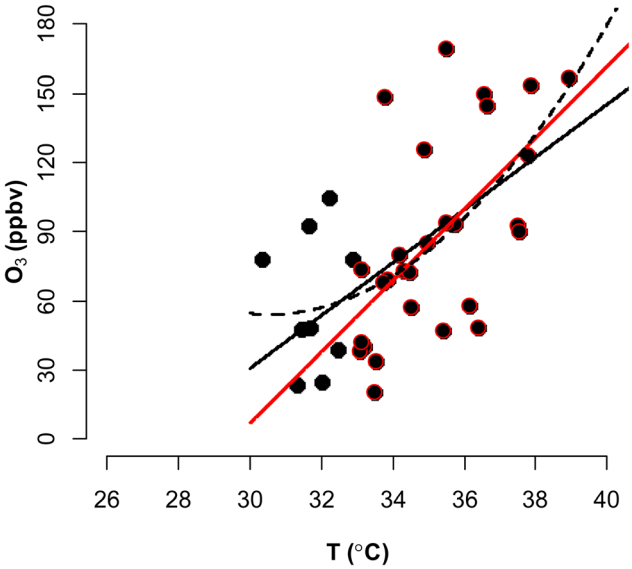

Fig. 2 The relationship between daily maximum O_3 and temperature (black solid circle). The "heatwave periods" (daily maximum temperature > 33 °C) are colored in red. Solid lines and dashed curve represent the linear (entire period (black solid line): $p < 0.05$, heatwave period (red solid line): $p < 0.05$) and quadratic regression (entire period (black dashed line): $p < 0.05$), respectively.

The O_3-climate penalty factor (CPF_{O_3}) was calculated based on the linear relationship ($CPF_{O_3\text{–L}}$) between the daily maximum O_3 concentration and the daily maximum temperature. The value was 11.5 ppbv °C^{-1} for the entire measurement period and 15.5 ppbv °C^{-1} during the heatwave (Table 1). The inclusion of extreme heatwave cases resulted in a higher $CPF_{O_3\text{–L}}$ for the entire measurement period compared to previous studies (~3 ppbv °C^{-1}).[16,17,19,23] Further the maximum daily 8 h average (MDA8) O_3 based $CPF_{O_3\text{–L}}$ also shows high value (8.1 ppbv °C^{-1}) during the whole periods, and it indicates that increase in O_3 concentration during the heatwave period may be appeared with the increase of temperature.

The acceleration of the O_3 increase at higher temperatures also can be attributed to the quadratic relationship between O_3 concentration and temperature. By applying a quadratic regression curve to the relationship between the daily maximum O_3 level and the daily maximum temperature, the coefficient of the quadratic function was calculated to represent the slope at each temperature point (eqn (1)). The derivative of $CPF_{O_3\text{–Q}}$ provides the $CPF_{O_3\text{–L}}$ as a function of temperature. Based on the measurement data, the following values were obtained: $b_0 = 1371.1$; $b_1\ i = -86.2$; $b_2 = 1.4$. Thus, the O_3–temperature dependency of the quadratic curve can be expressed by the following equation (eqn (3)):

$$\left.\frac{d[O_3]}{dT}\right|_{QR} = 2.8 \times T_{max} - 86.2 \quad (3)$$

The calculated coefficient of $CPF_{O_3\text{–Q}}$ (2.8) exceeded the upper boundary of the $CPF_{O_3\text{–Q}}$ range observed in previous studies (0.1–1.3).[26,27]

Open Access Article. Published on 06 Februarie 2026. Downloaded on 2026-05-11 6:57:09 nm..
This article is licensed under a Creative Commons Attribution-NonCommercial 3.0 Unported Licence.

Table 1 The climate penalty factor of O_3 (CPF_{O_3}) estimated from linear regression ($[O_3] = b_0 + b_1[T]$) and quadratic regression ($[O_3] = b_0 + b_1[T] + b_2[T]^2$) using the daily maximum O_3 and daily maximum temperature

Period	b_0	b_1	b_2	CPF_{O_3}
Heatwave (linear)	−458.0	15.5		15.5
Total (linear)	−313.2	11.5		11.5
Total (quadratic)	1371.1	−86.2	1.4	$2.8T - 86.2$

The $CPF_{O_3\_Q}$, obtained through quadratic regression, varied widely from 1 to 23 ppbv °C^{-1} above the observed inflection temperatures of over 30 °C (Tables S4 and S5). Interestingly, in previous studies in Seoul, temperatures exceeding 30 °C were identified as a prerequisite for elevated O_3 concentrations exceeding national air quality standards.[59,60] The $CPF_{O_3\_L}$ for the entire measurement period and the heatwave period aligned with the $CPF_{O_3\_Q}$ at temperatures of 35 and 36 °C, respectively. At the highest daily maximum temperature of 38.9 °C, the CPF_{O_3} was 22.8 ppbv °C^{-1}. These results highlight an accelerated O_3 increase during a heatwave in a megacity, which is appropriately represented by different values of O_3-temperature dependency at each temperature. This raises the following question: Why does the CPF_{O_3} be different with temperature?

The increase in O_3 resulting from a temperature increase can be elucidated through the discrete mechanisms governing O_3 enhancement. The CPF_{O_3} is attributed to variations in chemical reactions leading to O_3 production, emissions linked to biological activities or evaporation, and physical processes such as advection, diffusion, and vertical mixing, as represented by $\left.\frac{d[O_3]}{dT}\right|_{Chem}$, $\left.\frac{d[O_3]}{dT}\right|_{Emi}$, and $\left.\frac{d[O_3]}{dT}\right|_{Phy}$, respectively.[20]

The chemical term $\left(\left.\frac{d[O_3]}{dT}\right|_{Chem}\right)$ and emission term $\left(\left.\frac{d[O_3]}{dT}\right|_{Emi}\right)$ were initially computed together. Using the F0AM model, the change in O_3 levels in response to temperature and emission variations was simulated based on the several cases (M_T–M_S) described in Section 2.2. Using the measurement data and F0AM, the CPF_{O_3} attributable to chemistry and emissions was approximately 1.7–1.8 ppbv °C^{-1} (Fig. 3 and Table S7). When considering the uncertainties of temperature dependent emission factors from various VOCs emission sources that can be increased up to 6.7% °C^{-1}, it makes the variation in simulated $\left.\frac{d[O_3]}{dT}\right|_{Chem} + \left.\frac{d[O_3]}{dT}\right|_{Emi}$ value as 0.2 ppbv °C^{-1} (Table S7).[61] This upper bound of $\left.\frac{d[O_3]}{dT}\right|_{Chem} + \left.\frac{d[O_3]}{dT}\right|_{Emi}$ (~2 ppbv °C^{-1}) is near to the previous studies on the $CPF_{O_3\_L}$ (~3 ppbv °C^{-1});[21] however, it is lower than the $CPF_{O_3\_L}$ for the whole measurement period.

The physical term $\left(\left.\frac{d[O_3]}{dT}\right|_{Phy}\right)$ of eqn (2) primarily pertains to dynamic processes such as reinforced or decelerated long-range O_3 transport caused by the temperature increase, and consequently influenced surface O_3 levels. The transport of O_3 and stagnant weather conditions facilitate the formation and accumulation of O_3.[62,63]

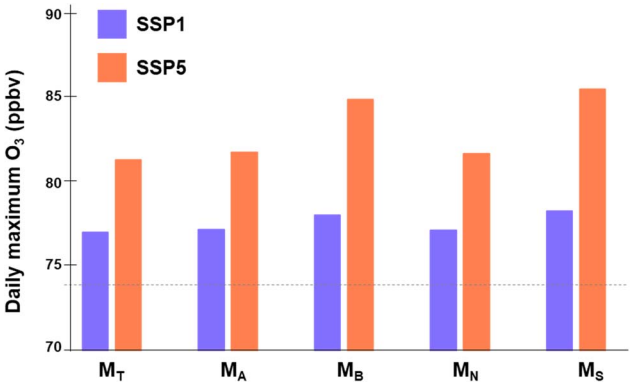

Fig. 3 Calculated daily maximum O_3 concentration during July to August. The gray dashed line indicates the modeled daily maximum O_3 concentration at the observed temperature ($\Delta T = 0$). Detail conditions of each '*M*' scenario are described in Table S7.

In this study, during the prolonged heatwave, blocking conditions played a crucial role in occurrence of heatwave over the Korean Peninsula. In Seoul, blocking conditions are commonly associated with synoptic atmospheric circulation, resulting in persistent anticyclonic or stagnant conditions.[30] This scenario was observed during the KORea-US Air Quality (KORUS-AQ) campaign accompanied by a significant elevation of O_3.[64] Similar to this previous study, in the present study, surface O_3 concentrations were significantly elevated under stagnant atmospheric conditions during heatwave periods in urban areas.

The boundary layer typically expands greatly under a persistent high-pressure system due to radiative heating. The daily evolution of this layer is thought to promote the photochemical production of O_3 through vertical turbulent mixing with the low NO_x concentration in the upper atmosphere above urban areas and also affects the surface O_3.[65–67] During the measurement period, the boundary layer height (BLH) expanded by 1500 m during the daytime, reaching its maximum between 14:00 and 17:00 local standard time (LST) before collapsing to nearly 500 m at nighttime, with its minimum occurring between 00:00 and 05:00 LST. Similarly, the maximum O_3 was observed when BLH was maximum and the minimum was observed when BLH was minimum. While BLH generally increased with temperature, the ratio of the daily range of BLH to that of temperature (ΔBLH/ΔT) remained relatively consistent during both the heatwave and non-heatwave periods (Fig. S5). In comparison, the ratio of the daily range of O_3 to that of BLH ($\Delta O_3/\Delta$BLH) was greater during heatwave periods than non-heatwave periods. As a result, the rate of change of O_3 with increasing temperature $\left(= \left.\frac{d[O_3]}{dT}\right|_{Phy}\right)$ was calculated to be 21.8% higher during the heatwave (10.6 ppbv °C^{-1}) than the non-heatwave period (8.7 ppbv °C^{-1}) (Table 2). Notably, both values of $\left.\frac{d[O_3]}{dT}\right|_{Phy}$ were significantly larger than those estimated for emissions and chemical processes (<2 ppbv °C^{-1}). For the heatwave period, the

 This journal is © The Royal Society of Chemistry 2026

Open Access Article. Published on 06 Februarie 2026. Downloaded on 2026-05-11 6:57:09 nm..
This article is licensed under a Creative Commons Attribution-NonCommercial 3.0 Unported Licence.

Table 2 Temperature dependency of boundary layer height (BLH) and the change of O_3 by a variation in BLH. All values were determined by the linear regression slope

	$\frac{dO_3}{dBLH}(=a)$ ($\times10^{-2}$ ppbv m^{-1})	$\frac{dBLH}{dT}(=b)$ ($\times10^{2}$ m °C^{-1})	$\frac{dO_3}{dT}(=a\times b)$ (ppbv °C^{-1})
Non-heatwave	4.5	1.9	8.7
Heatwave	5.2	2.1	10.6

discretization based on various measurement data resulted in a CPF_{O_3} $\left(=\left.\frac{d[O_3]}{dT}\right|_{Phy}+\left.\frac{d[O_3]}{dT}\right|_{Chem}+\left.\frac{d[O_3]}{dT}\right|_{Emi}\right)$ of 12.3–12.4 ppbv °C^{-1}, which is similar to the $CPF_{O_3\_L}$ in heatwave periods of 15.5 ppbv °C^{-1}. During the heatwave, $\left.\frac{d[O_3]}{dT}\right|_{Phy}$ was about five times higher than $\left(\left.\frac{d[O_3]}{dT}\right|_{Chem}+\left.\frac{d[O_3]}{dT}\right|_{Emi}\right)$, indicating that physical processes were the primary drivers of the accelerated O_3 enhancement during the heatwave.

3.2. Vertical mixing as a physical driver of accelerated surface O_3 enhancement

In NO_x-saturated regions, model calculations demonstrate that surface O_3 is titrated by NO_x in the early morning and accumulates in the afternoon.[68] Recent studies conducted in tall towers have demonstrated that free convection and vertical mixing facilitate efficient O_3 formation, leading to elevated O_3 and PAN concentrations at higher altitudes.[69,70] This is consistent with our results that, in discretization methods, physical processes exert the most significant influence on CPF_{O_3}.

The degree of atmospheric vertical mixing within the boundary layer can be expressed by the turbulent diffusion coefficient (k_z),[71] which is calculated using the following equations for $z < L$ (eqn (4)):[72]

$$k_z(z) = k_z(L) + \left(\frac{L-z}{L-L_0}\right)^2 \times \left[k_z(L_0) - k_z(L) + (z-L_0)\left(\frac{k_z(L_0)}{L_0} + 2\frac{k_z(L_0)-k_z(L)}{L-L_0}\right)\right] \quad (4)$$

where $k_z(L)$ is the turbulent diffusivity above the boundary layer (=1.0 cm^2 s^{-1}), z is the height, L is the height of the boundary layer, L_0 is the height of the surface layer ($\sim0.1L$), and $k_z(L_0)$ is the turbulent diffusivity at the top of the surface layer (Text S1). Here, k_z is presented with the measured BLH for the heatwave and non-heatwave periods (Fig. 4). k_z exhibited higher values during the heatwave, coinciding with the earlier development and greater expansion of the boundary layer compared to the non-heatwave period. These trends in k_z and BLH were mirrored in the diurnal variations of O_3 for the two cases shown in Fig. S6.

Similar to the variation of k_z, the diurnal variation of O_3 simulated using the WRF-Chem model also showed large differences between the heatwave and non-heatwave periods (Fig. 5). The diurnal evolution of O_3 was strongly correlated with changes in BLH, with O_3 levels remaining low (below 10 ppbv) under a stable boundary layer until early morning and then rapidly increasing with the rise in BLH. The two cases exhibited sharply contrast in change of O_3, that the morning upward and afternoon downward gradient in O_3 concentration was more pronounced during the heatwave. These highlight the influence of physical terms in the CPF_{O_3} equation, which were estimated from the measurements of reactive gases including O_3, nitrogen oxide species, and VOCs, and BLH based on discretization methods.

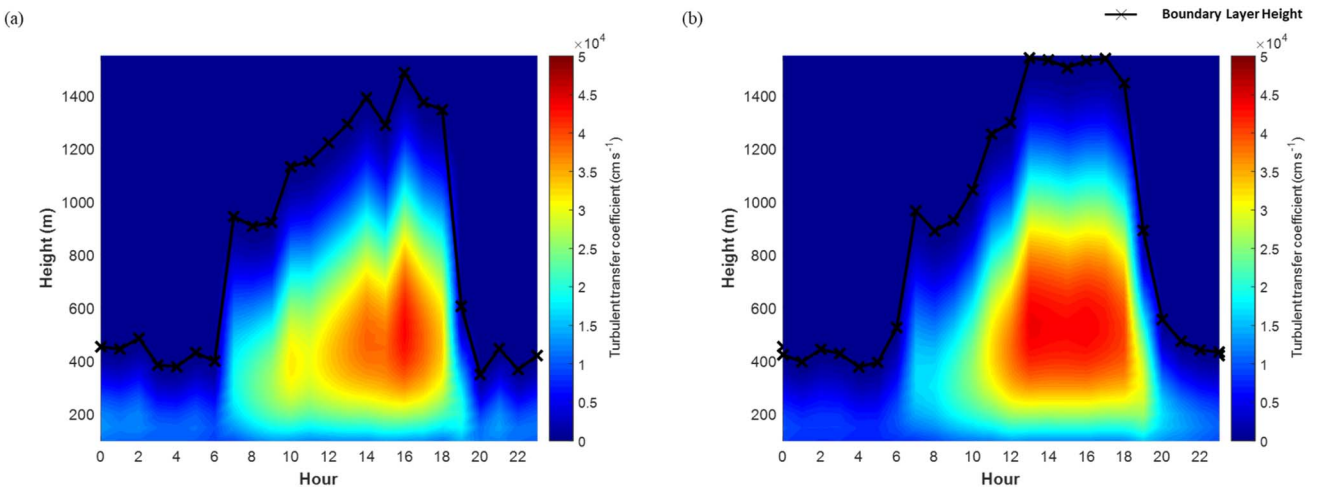

Fig. 4 Turbulent transfer coefficient (k_z) based on the wind speed at the top of surface layer during (a) non-heatwave period and (b) heatwave period.

Open Access Article. Published on 06 Februarie 2026. Downloaded on 2026-05-11 6:57:09 nm..
This article is licensed under a Creative Commons Attribution-NonCommercial 3.0 Unported Licence.

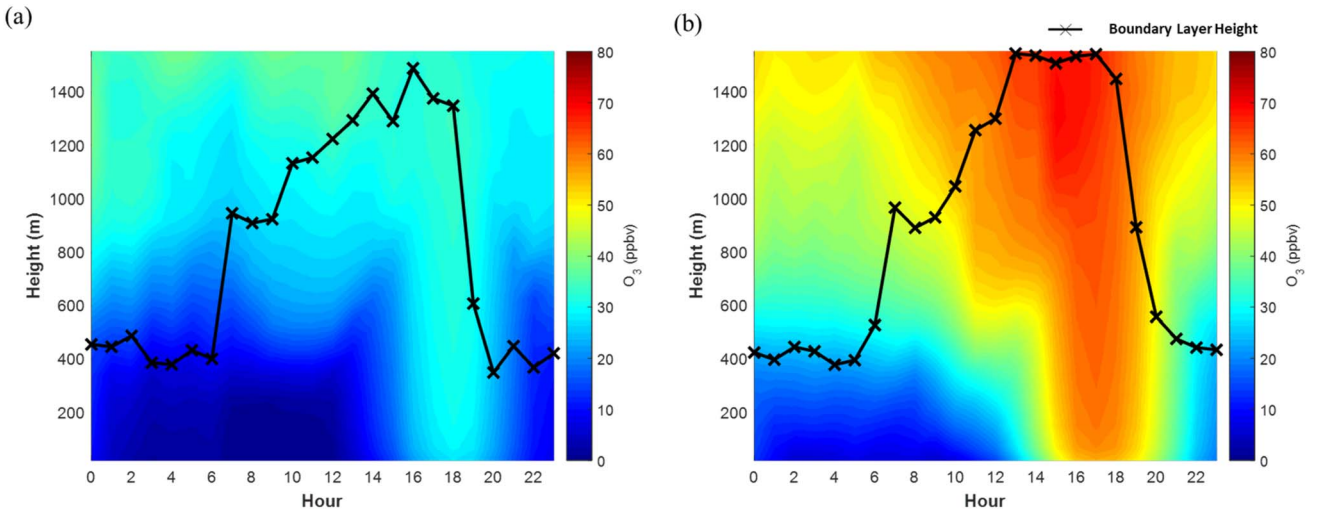

Fig. 5 Diurnal-vertical variations in O_3 concentrations during the (a) non-heatwave and (b) heatwave periods in Seoul simulated by WRF-Chem v3.9.1.

3.3. Ozone production efficiency

In a megacity such as Seoul, NO_2 levels typically reach their minimum in the afternoon, coinciding with the O_3 peak.[64] However, it was not observed in this study. Instead, NO_2 concentration remained high in the afternoon, especially when the boundary layer was most expanded (Fig. 6(a) and (b)), indicating a rapid chemical cycling of nitrogen oxides. Based on the O_3 production ($=P(O_3)$) and loss of NO_x ($=L(NO_x)$) chemistry, the ozone production efficiency (OPE) was obtained using

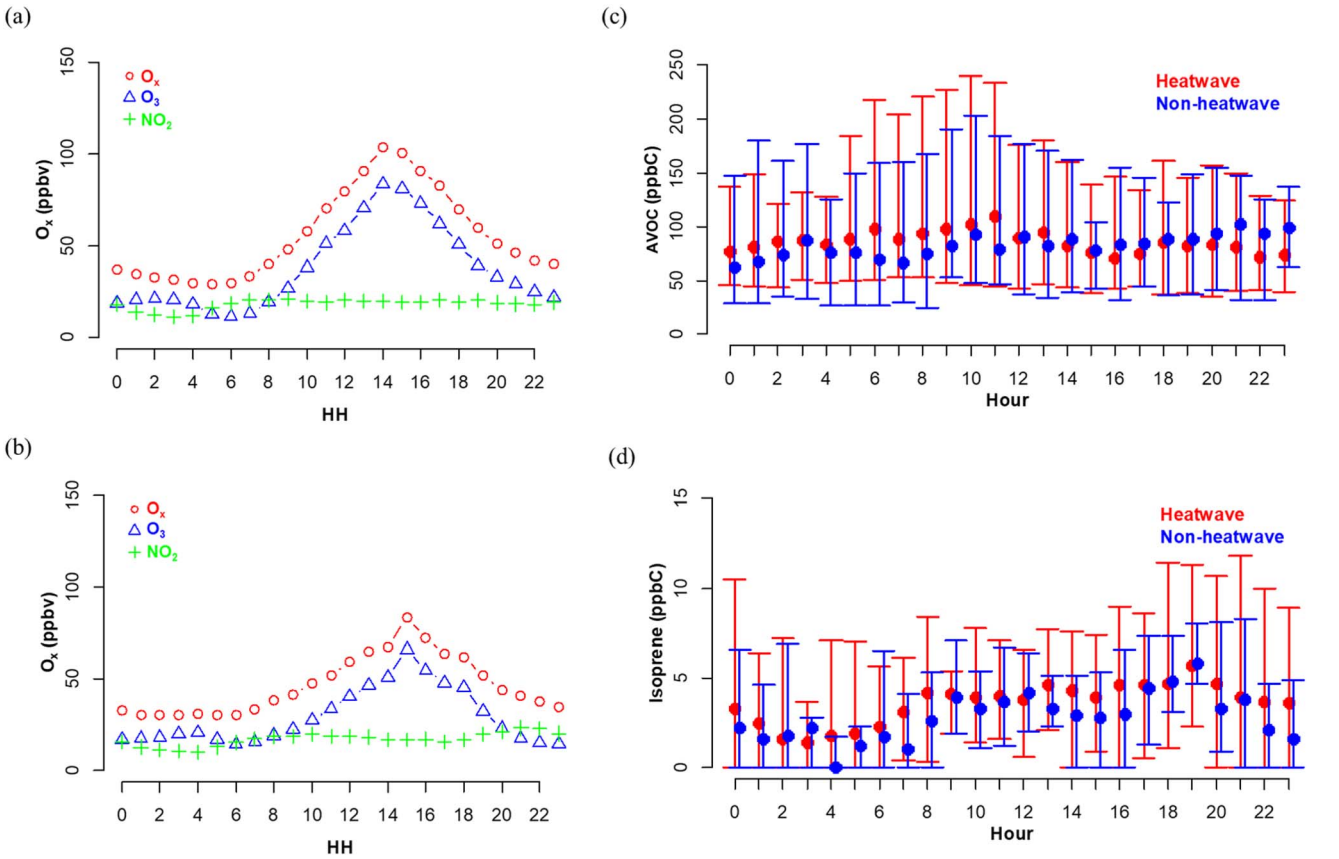

Fig. 6 (Left panels) Diurnal variation of O_x, O_3, and NO_2 during the (a) heatwave period and (b) non-heatwave period, respectively. (Right panels) Diurnal variation of (c) AVOCs and (d) isoprene during the heatwave and non-heatwave period, respectively. Each symbol and solid bar imply averaged values and their standard deviations.

 This journal is © The Royal Society of Chemistry 2026

Open Access Article. Published on 06 Februarie 2026. Downloaded on 2026-05-11 6:57:09 nm..
This article is licensed under a Creative Commons Attribution-NonCommercial 3.0 Unported Licence.

the level of O_x (=O_3 + NO_2) and NO_z, where $[NO_2] + [NO_z] \ll [O_3]$[73,74] (eqn (5)–(7)).

$$P(O_3) = k_{HO_2+NO}[HO_2][NO] + \sum_i k_{RO_{2,i}+NO}[RO_{2,i}][NO] \approx [O_x] \quad (5)$$

$$L(NO_x) = k_{OH+NO_2}[OH][NO_2] + \sum_i k_{RO_{2,i}+NO}[RO_{2,i}][NO] + \sum_i k_{RCO_{3,i}+NO_2}[RCO_{3,i}][NO_2] - \sum_i k_{RCO_3NO_{2,i}}[RCO_3NO_{2,i}] \approx [NO_z] \quad (6)$$

$$OPE = \frac{P(O_3)}{L(NO_x)} \approx \frac{[O_x]}{[NO_z]} \quad (7)$$

Using measurements of the nitrogen oxide species HONO, PAN, and HNO_3, the OPE, represented by the ratio of O_x (O_3 + NO_2) to NO_z (=PAN + HONO + HNO_3), was compared between the heatwave and non-heatwave periods. The OPE during the heatwave was 18.9, while it was 16.4 during the non-heatwave period (Fig. 7), with both values being higher than the range of 3–8 reported in previous studies that heatwave had not been occurred.[73,74] Hence, the OPE likely played a pivotal role in enhancing O_3 levels in the summer heatwave periods.[24,67]

The formation of O_3 was found to be sensitive to the concentrations of VOCs under NO_x-saturated conditions. During the heatwave, anthropogenic VOCs (AVOC) and isoprene mixing ratios were larger than in the non-heatwave period, correlated with an increase in daytime temperature (Fig. 6(c) and (d)). Particularly, in the morning, AVOC concentrations were consistently elevated during the heatwave period compared to the non-heatwave period (2.7% $°C^{-1}$), surpassing the typical temperature dependency of VOCs observed in previous studies (1.3% $°C^{-1}$).[42] This observation aligns with VOC patterns previously observed in Seoul, highlighting the fugitive emissions of AVOCs at elevated temperatures.[43]

During the heatwave, the mean isoprene concentration increased by approximately four times (10.3% $°C^{-1}$), more than the increase in AVOCs. However, isoprene emissions are constrained at temperatures above the threshold of plant growth.[75] On the other hand, AVOCs from fugitive emissions are likely to continue to increase with temperature. But these increase in VOCs only can contribute to the 4–5 ppbv $°C^{-1}$ of CPF_{O_3}, and it is hard to fully explain the increase of CPF_{O_3} during the heatwave period through only the increase in VOC concentration. Consequently, the heightened OPE, together with a change of boundary-layer related processes and increased VOC levels, was found to be a crucial physical factor in the significantly elevated O_3 concentrations during the heatwave. The results show that prolonged heatwaves likely promote deep vertical mixing, thereby increasing O_3 production by enhanced OPE due to increased fugitive emissions of VOCs. These findings underscore the importance of focusing on AVOCs to mitigate the accelerated O_3 increase in urban areas during heatwaves.

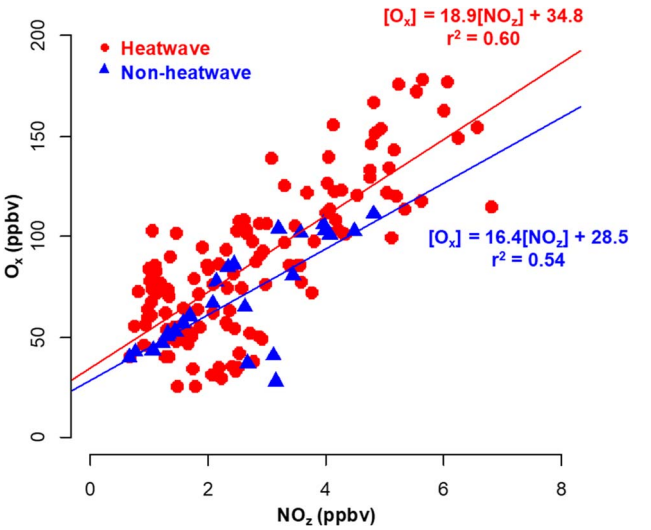

Fig. 7 The ozone production efficiency (OPE) as the ratio of O_x to NO_z during the midday (10–17 LST) for heatwave (red) and non-heatwave (blue) periods.

4. Conclusions

This study revealed a significant O_3-climate penalty in urban Seoul during short-term heatwave periods in summer 2018, surpassing the values reported in previous long-term observations, with the rate of change of the penalty (penalty factor) increasing with temperature. Measurements and model simulations underscored the significance of dynamic boundary-layer processes as a key pathway for O_3 enhancement. However, the effect of the intricate interplay between dynamic processes and chemical reactions on change of O_3-climate penalty factor remains incompletely understood.

These findings suggest that the increasing frequency of heatwaves due to global warming could lead to rapid O_3 increases in megacities, characterized by high levels of NO_x and VOCs due to vehicle emissions. Efficient O_3 production during heatwaves, facilitated by vertical mixing and fueled by increased fugitive emissions of VOCs, emphasizes the need to reduce AVOCs in megacity and its surrounding areas to mitigate the accelerating increase in O_3 observed during heatwaves. These dynamic processes combined with the change of chemical change can lead to the non-linear increase of O_3 climate penalty not only in the megacity, but further expanded to the metropolitan region especially during the warm season, which was reported as a critical problem in global ozone pollution.[76] Therefore, this study establishes a framework for analyzing O_3 enhancement mechanisms and estimating CPF_{O_3} during future heatwaves, providing insights for effective pollutant reduction policies under climate change.

Author contributions

JG and ML conceptualize and design this research. JG, MP, SK, and HR contributed to the data collection. JG, CK, JK, and HL conducted the modelling and contributed to the analysis. All authors contributed to the interpretation of the results and manuscript writing.

Open Access Article. Published on 06 Februarie 2026. Downloaded on 2026-05-11 6:57:09 nm..
This article is licensed under a Creative Commons Attribution-NonCommercial 3.0 Unported Licence.

Conflicts of interest

The authors declare no competing interests.

Data availability

Data for this article, including the observation data, are available at the repository (https://zenodo.org/records/11045153).[77]

Supplementary information (SI) is available. See DOI: https://doi.org/10.1039/d5em00629e.

Acknowledgements

This research was supported by National Research Foundation of Republic of Korea (2020R1A2C3014592) and Seoul Metropolitan Government (2019030A3C700). This study was also supported by the National Research Foundation of Korea (NRF) grant funded by the Korea government (MSIT) (RS-2025-00573406).

References

1 IPCC, in *Climate Change 2023: Synthesis Report. Contribution of Working Groups I, II and III to the Sixth Assessment Report of the Intergovernmental Panel on Climate Change*, 2023.
2 NIMS, *Global Climate Change Prospect Report*, National Institute of Meteorological Sciences, 2020.
3 B. C. O'Neill, C. Tebaldi, D. P. van Vuuren, V. Eyring, P. Friedlingstein, G. Hurtt, R. Knutti, E. Kriegler, J.-F. Lamarque and J. Lowe, The scenario model intercomparison project (ScenarioMIP) for CMIP6, *Geosci. Model Dev.*, 2016, **9**, 3461–3482.
4 B. C. O'Neill, E. Kriegler, K. Riahi, K. L. Ebi, S. Hallegatte, T. R. Carter, R. Mathur and D. P. van Vuuren, A new scenario framework for climate change research: the concept of shared socioeconomic pathways, *Clim. Change*, 2014, **122**, 387–400.
5 P. A. Dirmeyer, G. Balsamo, E. M. Blyth, R. Morrison and H. M. Cooper, Land-atmosphere interactions exacerbated the drought and heatwave over northern Europe during summer 2018, *AGU Adv.*, 2021, **2**, e2020AV000283.
6 S. Undorf, K. Allen, J. Hagg, S. Li, F. Lott, M. J. Metzger, S. Sparrow and S. Tett, Learning from the 2018 heatwave in the context of climate change: Are high-temperature extremes important for adaptation in Scotland?, *Environ. Res. Lett.*, 2020, **15**, 034051.
7 Y. Qian, H. Murakami, P.-c. Hsu and S. Kapnick, Effects of anthropogenic forcing and natural variability on the 2018 heatwave in Northeast Asia, *Bull. Am. Meteorol. Soc.*, 2020, **101**, S77–S82.
8 J. Zhang, Y. Gao, K. Luo, L. R. Leung, Y. Zhang, K. Wang and J. Fan, Impacts of compound extreme weather events on ozone in the present and future, *Atmos. Chem. Phys.*, 2018, **18**, 9861–9877.
9 A. Pyrgou, P. Hadjinicolaou and M. Santamouris, Enhanced near-surface ozone under heatwave conditions in a Mediterranean island, *Sci. Rep.*, 2018, **8**, 9191.
10 X. Pu, T. Wang, X. Huang, D. Melas, P. Zanis, D. Papanastasiou and A. Poupkou, Enhanced surface ozone during the heat wave of 2013 in Yangtze River Delta region, China, *Sci. Total Environ.*, 2017, **603**, 807–816.
11 D. T. Shindell, J.-F. Lamarque, M. Schulz, M. Flanner, C. Jiao, M. Chin, P. Young, Y. H. Lee, L. Rotstayn and N. Mahowald, Radiative forcing in the ACCMIP historical and future climate simulations, *Atmos. Chem. Phys.*, 2013, **13**, 2939–2974.
12 D. Stevenson, P. Young, V. Naik, J.-F. Lamarque, D. T. Shindell, A. Voulgarakis, R. B. Skeie, S. B. Dalsoren, G. Myhre and T. K. Berntsen, Tropospheric ozone changes, radiative forcing and attribution to emissions in the Atmospheric Chemistry and Climate Model Intercomparison Project (ACCMIP), *Atmos. Chem. Phys.*, 2013, **13**, 3063–3085.
13 G. Myhre, W. Aas, R. Cherian, W. Collins, G. Faluvegi, M. Flanner, P. Forster, Ø. Hodnebrog, Z. Klimont and M. T. Lund, Multi-model simulations of aerosol and ozone radiative forcing due to anthropogenic emission changes during the period 1990–2015, *Atmos. Chem. Phys.*, 2017, **17**, 2709–2720.
14 P. S. Monks, A. Archibald, A. Colette, O. Cooper, M. Coyle, R. Derwent, D. Fowler, C. Granier, K. S. Law and G. Mills, Tropospheric ozone and its precursors from the urban to the global scale from air quality to short-lived climate forcer, *Atmos. Chem. Phys.*, 2015, **15**, 8889–8973.
15 S. Wu, L. J. Mickley, E. M. Leibensperger, D. J. Jacob, D. Rind and D. G. Streets, Effects of 2000–2050 global change on ozone air quality in the United States, *J. Geophys. Res.: Atmos.*, 2008, **113**, D06302.
16 B. J. Bloomer, J. W. Stehr, C. A. Piety, R. J. Salawitch and R. R. Dickerson, Observed relationships of ozone air pollution with temperature and emissions, *Geophys. Res. Lett.*, 2009, **36**, L09803.
17 N. Otero, J. Sillmann, K. A. Mar, H. W. Rust, S. Solberg, C. Andersson, M. Engardt, R. Bergström, B. Bessagnet and A. Colette, A multi-model comparison of meteorological drivers of surface ozone over Europe, *Atmos. Chem. Phys.*, 2018, **18**, 12269–12288.
18 C. G. Nolte, T. L. Spero, J. H. Bowden, M. C. Sarofim, J. Martinich and M. S. Mallard, Regional temperature-ozone relationships across the US under multiple climate and emissions scenarios, *J. Air Waste Manage. Assoc.*, 2021, **71**, 1251–1264.
19 C. Gong, Y. Wang, H. Liao, P. Wang, J. Jin and Z. Han, Future Co-Occurrences of Hot Days and Ozone-Polluted Days Over China Under Scenarios of Shared Socioeconomic Pathways Predicted Through a Machine-Learning Approach, *Earth's Future*, 2022, **10**, e2022EF002671.
20 D. Rasmussen, J. Hu, A. Mahmud and M. J. Kleeman, The ozone–climate penalty: past, present, and future, *Environ. Sci. Technol.*, 2013, **47**, 14258–14266.
21 S. Zhao, A. J. Pappin, S. Morteza Mesbah, J. Joyce Zhang, N. L. MacDonald and A. Hakami, Adjoint estimation of ozone climate penalties, *Geophys. Res. Lett.*, 2013, **40**, 5559–5563.

 This journal is © The Royal Society of Chemistry 2026

Open Access Article. Published on 06 Februarie 2026. Downloaded on 2026-05-11 6:57:09 nm..
This article is licensed under a Creative Commons Attribution-NonCommercial 3.0 Unported Licence.

22 W. C. Porter and C. L. Heald, The mechanisms and meteorological drivers of the summertime ozone–temperature relationship, *Atmos. Chem. Phys.*, 2019, **19**, 13367–13381.
23 J. M. Johansson, Å. K. Watne, P. E. Karlsson, G. P. Karlsson, H. Danielsson, C. Andersson and H. Pleijel, The European heat wave of 2018 and its promotion of the ozone climate penalty in southwest Sweden, *Boreal Environ. Res.*, 2020, **25**, 1.
24 W. Zhao, G. Tang, H. Yu, Y. Yang, Y. Wang, L. Wang, J. An, W. Gao, B. Hu and M. Cheng, Evolution of boundary layer ozone in Shijiazhuang, a suburban site on the North China Plain, *J. Environ. Sci.*, 2019, **83**, 152–160.
25 S. E. Pusede, A. L. Steiner and R. C. Cohen, Temperature and recent trends in the chemistry of continental surface ozone, *Chem. Rev.*, 2015, **115**, 3898–3918.
26 P. Jing, Z. Lu and A. L. Steiner, The ozone-climate penalty in the Midwestern US, *Atmos. Environ.*, 2017, **170**, 130–142.
27 Y. Gu, K. Li, J. Xu, H. Liao and G. Zhou, Observed dependence of surface ozone on increasing temperature in Shanghai, China, *Atmos. Environ.*, 2020, **221**, 117108.
28 X. Zhou, M. Li, X. Huang, T. Liu, H. Zhang, X. Qi, Z. Wang, Y. Qin, G. Geng and J. Wang, Urban meteorology–chemistry coupling in compound heat–ozone extremes, *Nat. Cities*, 2025, 1–10.
29 Korea Meteorological Administration (KMA), *2018 Meteorological Yearbook*, 2019, pp. 1–431.
30 K.-J. Ha, J.-H. Yeo, Y.-W. Seo, E.-S. Chung, J.-Y. Moon, X. Feng, Y.-W. Lee and C.-H. Ho, What caused the extraordinarily hot 2018 summer in Korea?, *J. Meteorol. Soc. Jpn. Ser. II*, 2020, 153–167.
31 D. Yoon, D.-H. Cha, M.-I. Lee, K.-H. Min, J. Kim, S.-Y. Jun and Y. Choi, Recent changes in heatwave characteristics over Korea, *Clim. Dyn.*, 2020, **55**, 1685–1696.
32 H.-D. Lee, K.-H. Min, J.-H. Bae and D.-H. Cha, Characteristics and comparison of 2016 and 2018 heat wave in Korea, *Atmosphere*, 2020, **30**, 1–15.
33 Seoul Metropolitan Government Research Institute of Public Health and Environment (SMGRIPHE), *2018 Seoul Air Quality Assessment Report*, 2019, pp. 1–102.
34 G. Lee, Y. Jang, H. Lee, J.-S. Han, K.-R. Kim and M. Lee, Characteristic behavior of peroxyacetyl nitrate (PAN) in Seoul megacity, Korea, *Chemosphere*, 2008, **73**, 619–628.
35 J. Gaffney, R. Bornick, Y.-H. Chen and N. Marley, Capillary gas chromatographic analysis of nitrogen dioxide and PANs with luminol chemiluminescent detection, *Atmos. Environ.*, 1998, **32**, 1445–1454.
36 J. Gil, J. Son, S. Kang, J. Park, M. Lee, E. Jeon and M. Shim, HONO measurement in Seoul during Summer 2018 and its Impact on Photochemistry, *J. Korean Soc. Atmos. Environ.*, 2020, **36**, 579–588.
37 Vaisala, *User's Guide, Vaisala Ceilometer CL51*, Helsinki, Finland, 2010.
38 C. Werner, Doppler Wind Lidar, *Lidar: Range-Resolved Optical Remote Sensing of the Atmosphere*, 2005.
39 RPG, *RPG: Instrument Operation and Software Guide, Operational Principles and Software Description for RPG Standard Single Polarization Radiometer (G4 Series)*, 2015, p. 170.
40 J.-S. Min, M.-S. Park, J.-H. Chae and M. Kang, Integrated System for Atmospheric Boundary Layer Height Estimation (ISABLE) using a ceilometer and microwave radiometer, *Atmos. Meas. Tech.*, 2020, **13**, 6965–6987.
41 G. M. Wolfe, M. R. Marvin, S. J. Roberts, K. R. Travis and J. Liao, The framework for 0-D atmospheric modeling (F0AM) v3.1, *Geosci. Model Dev.*, 2016, **9**, 3309.
42 J. I. Rubin, A. J. Kean, R. A. Harley, D. B. Millet and A. H. Goldstein, Temperature dependence of volatile organic compound evaporative emissions from motor vehicles, *J. Geophys. Res.: Atmos.*, 2006, **111**, D03305.
43 S. Kang, J.-A. Kim, M. Lee, J. Park, E. Jeon, M. Shim and Y. Shin, An analysis of the temporal variability in volatile organic compounds (VOCs) within megacity Seoul and an identification of their sources, *Atmos. Pollut. Res.*, 2022, **13**, 101338.
44 L. K. Emmons, S. Walters, P. G. Hess, J.-F. Lamarque, G. G. Pfister, D. Fillmore, C. Granier, A. Guenther, D. Kinnison and T. Laepple, Description and evaluation of the Model for Ozone and Related chemical Tracers, version 4 (MOZART-4), *Geosci. Model Dev.*, 2010, **3**, 43–67.
45 A. Guenther, T. Karl, P. Harley, C. Wiedinmyer, P. Palmer and C. Geron, Estimates of global terrestrial isoprene emissions using MEGAN (Model of Emissions of Gases and Aerosols from Nature), *Atmos. Chem. Phys.*, 2006, **6**, 3181–3210.
46 A. L. Steiner, A. J. Davis, S. Sillman, R. C. Owen, A. M. Michalak and A. M. Fiore, Observed suppression of ozone formation at extremely high temperatures due to chemical and biophysical feedbacks, *Proc. Natl. Acad. Sci. U. S. A.*, 2010, **107**, 19685–19690.
47 W. C. Skamarock and J. B. Klemp, A time-split nonhydrostatic atmospheric model for weather research and forecasting applications, *J. Comput. Phys.*, 2008, **227**, 3465–3485.
48 G. A. Grell, S. E. Peckham, R. Schmitz, S. A. McKeen, G. Frost, W. C. Skamarock and B. Eder, Fully coupled "online" chemistry within the WRF model, *Atmos. Environ.*, 2005, **39**, 6957–6975.
49 NCEP, NOAA, and USDC, *NCEP FNL Operational Model Global Tropospheric Analyses, Continuing from July 1999*, Research Data Archive at the National Center for Atmospheric Research, Computational and Information Systems Laboratory, updated daily, 2000, DOI: 10.5065/D6M043C6.
50 W. R. Stockwell, F. Kirchner, M. Kuhn and S. Seefeld, A new mechanism for regional atmospheric chemistry modeling, *J. Geophys. Res.: Atmos.*, 1997, **102**, 25847–25879.
51 R. Ahmadov, S. McKeen, A. Robinson, R. Bahreini, A. Middlebrook, J. De Gouw, J. Meagher, E. Y. Hsie, E. Edgerton and S. Shaw, A volatility basis set model for summertime secondary organic aerosols over the eastern United States in 2006, *J. Geophys. Res.: Atmos.*, 2012, **117**, D06301.

Open Access Article. Published on 06 Februarie 2026. Downloaded on 2026-05-11 6:57:09 nm..
This article is licensed under a Creative Commons Attribution-NonCommercial 3.0 Unported Licence.

52 R. J. Park, Y. J. Oak, L. K. Emmons, C.-H. Kim, G. G. Pfister, G. R. Carmichael, P. E. Saide, S.-Y. Cho, S. Kim and J.-H. Woo, Multi-model intercomparisons of air quality simulations for the KORUS-AQ campaign, *Elementa*, 2021, **9**, 00139.
53 P. Bloomfield, J. A. Royle, L. J. Steinberg and Q. Yang, Accounting for meteorological effects in measuring urban ozone levels and trends, *Atmos. Environ.*, 1996, **30**, 3067–3077.
54 L. Carro-Calvo, C. Ordóñez, R. García-Herrera and J. L. Schnell, Spatial clustering and meteorological drivers of summer ozone in Europe, *Atmos. Environ.*, 2017, **167**, 496–510.
55 T.-M. Fu and H. Tian, Climate Change Penalty to Ozone Air Quality: Review of Current Understandings and Knowledge Gaps, *Curr. Pollut. Rep.*, 2019, **5**, 159–171.
56 Y. F. Lam, H. M. Cheung and C. C. Ying, Impact of tropical cyclone track change on regional air quality, *Sci. Total Environ.*, 2018, **610**, 1347–1355.
57 A. Ito, S. Sillman and J. E. Penner, Global chemical transport model study of ozone response to changes in chemical kinetics and biogenic volatile organic compounds emissions due to increasing temperatures: Sensitivities to isoprene nitrate chemistry and grid resolution, *J. Geophys. Res.: Atmos.*, 2009, **114**, D09301.
58 L. Camalier, W. Cox and P. Dolwick, The effects of meteorology on ozone in urban areas and their use in assessing ozone trends, *Atmos. Environ.*, 2007, **41**, 7127–7137.
59 J. Han, H. Kim, M. Lee, S. Kim and S. Kim, Photochemical air pollution of Seoul in the last three decades, *J. Korean Soc. Atmos. Environ.*, 2013, **29**, 390–406.
60 H. C. Kim, D. Lee, F. Ngan, B.-U. Kim, S. Kim, C. Bae and J.-H. Yoon, Synoptic weather and surface ozone concentration in South Korea, *Atmos. Environ.*, 2021, **244**, 117985.
61 M. Qin, Y. She, M. Wang, H. Wang, Y. Chang, Z. Tan, J. An, J. Huang, Z. Yuan and J. Lu, Increased urban ozone in heatwaves due to temperature-induced emissions of anthropogenic volatile organic compounds, *Nat. Geosci.*, 2025, **18**, 50–56.
62 J. Seo, D.-S. R. Park, J. Y. Kim, D. Youn, Y. B. Lim and Y. Kim, Effects of meteorology and emissions on urban air quality: a quantitative statistical approach to long-term records (1999–2016) in Seoul, South Korea, *Atmos. Chem. Phys.*, 2018, **18**, 16121–16137.
63 E. M. Oswald, L.-A. Dupigny-Giroux, E. M. Leibensperger, R. Poirot and J. Merrell, Climate controls on air quality in the Northeastern US: An examination of summertime ozone statistics during 1993–2012, *Atmos. Environ.*, 2015, **112**, 278–288.
64 H. Kim, J. Gil, M. Lee, J. Jung, A. Whitehill, J. Szykman, G. Lee, D.-S. Kim, S. Cho and J.-Y. Ahn, Factors controlling surface ozone in the Seoul Metropolitan Area during the KORUS-AQ campaign, *Elementa*, 2020, **8**, 46.
65 X.-B. Li, B. Yuan, S. Wang, C. Wang, J. Lan, Z. Liu, Y. Song, X. He, Y. Huangfu and C. Pei, Variations and sources of volatile organic compounds (VOCs) in urban region: insights from measurements on a tall tower, *Atmos. Chem. Phys.*, 2022, **22**, 10567–10587.
66 N. Otero, H. W. Rust and T. Butler, Temperature dependence of tropospheric ozone under NOx reductions over Germany, *Atmos. Environ.*, 2021, **253**, 118334.
67 G. Tang, Y. Liu, X. Huang, Y. Wang, B. Hu, Y. Zhang, T. Song, L. Xiaolan, S. Wu and Q. Li, Aggravated ozone pollution in the strong free convection boundary layer, *Sci. Total Environ.*, 2021, 147740.
68 J. H. Crawford, J.-Y. Ahn, J. Al-Saadi, L. Chang, L. K. Emmons, J. Kim, G. Lee, J.-H. Park, R. J. Park and J. H. Woo, The Korea–United States air quality (KORUS-AQ) field study, *Elementa*, 2021, **9**, 00163.
69 Q. Yao, Z. Ma, J. Liu, Y. Qiu, T. Hao, L. Yao, J. Ding, Y. Tang, Z. Cai and S. Han, Effects of Meteorological Factors on the Vertical Distribution of Peroxyacetyl Nitrate in Autumn in Tianjin, *Aerosol Air Qual. Res.*, 2022, **22**, 220226.
70 Y. Qiu, W. Lin, K. Li, L. Chen, Q. Yao, Y. Tang and Z. Ma, Vertical characteristics of peroxyacetyl nitrate (PAN) from a 250-m tower in northern China during September 2018, *Atmos. Environ.*, 2019, **213**, 55–63.
71 R. A. Pielke and Y. Mahrer, Representation of the heated planetary boundary layer in mesoscale models with coarse vertical resolution, *J. Atmos. Sci.*, 1975, **32**, 2288–2308.
72 M. Herrmann, L. Cao, H. Sihler, U. Platt and E. Gutheil, On the contribution of chemical oscillations to ozone depletion events in the polar spring, *Atmos. Chem. Phys.*, 2019, **19**, 10161–10190.
73 W. Zhou, D. Cohan and B. Henderson, Slower ozone production in Houston, Texas following emission reductions: evidence from Texas Air Quality Studies in 2000 and 2006, *Atmos. Chem. Phys.*, 2014, **14**, 2777–2788.
74 C. C. K. Chou, C. Y. Tsai, C. J. Shiu, S. C. Liu and T. Zhu, Measurement of NOy during campaign of air quality research in Beijing 2006 (CAREBeijing-2006): Implications for the ozone production efficiency of NOx, *J. Geophys. Res.: Atmos.*, 2009, **114**, D00G01.
75 B. Rasulov, K. Hüve, I. Bichele, A. Laisk and Ü. Niinemets, Temperature response of isoprene emission in vivo reflects a combined effect of substrate limitations and isoprene synthase activity: a kinetic analysis, *Plant Physiol.*, 2010, **154**, 1558–1570.
76 X. Lyu, K. Li, H. Guo, L. Morawska, B. Zhou, Y. Zeren, F. Jiang, C. Chen, A. H. Goldstein and X. Xu, A synergistic ozone-climate control to address emerging ozone pollution challenges, *One Earth*, 2023, **6**, 964–977.
77 J. Gil, Seoul ground observation data in 2018 summer, *Dataset*, 2024, DOI: 10.5281/zenodo.11045153.

 This journal is © The Royal Society of Chemistry 2026